AIAA JOURNAL
Vol. 47, No. 1, January 2009

Algorithm for the Nonlinear Propagation of Broadband Jet Noise

Swati Saxena* and Philip J. Morris†
Pennsylvania State University, University Park, Pennsylvania 16802
and
K. Viswanathan‡
The Boeing Company, Seattle, Washington 98124

DOI: 10.2514/1.38122

A frequency-domain algorithm for nonlinear noise propagation is presented. The propagation of noise generated by very high-speed jets exhibits nonlinear effects. This nonlinear behavior, which includes the transfer of energy to high frequencies, is captured in the present algorithm. The generalized nonlinear Burgers equation, which includes atmospheric absorption and dissipation, is solved for the pressure signal in the frequency domain. The results are then obtained as a function of time. A test case of a sinusoidal wave is considered, and the results are compared with the existing analytical Blackstock Bridging Function and Fubini solutions. The predicted results of the sinusoidal wave case agree fairly well with the analytical results. Jet noise data from the Boeing Low Speed Aeroacoustic Facility are used for the broadband noise prediction. The experimental and predicted power spectral density plots are compared for microphones at different radial locations. The predicted results are in good agreement with the experimental results at all the microphone locations, and the power spectral density plots show a lift at high frequencies due to the nonlinear steepening of the waves. The skewness of the experimental and predicted signal is discussed for the Boeing data. Full-scale data acquired during a tie-down test of the F/A-18E are propagated using the nonlinear and linear predictions, and the differences in the results are discussed. Ground reflection effects are then presented for both the Boeing and F/A-18E engine data.

Nomenclature

A	=	amplitude of complex Fourier transform of pressure
c	=	ambient speed of sound
f	=	frequency of the acoustic signal
f_o	=	fundamental frequency of the sinusoidal wave
i	=	$\sqrt{-1}$
k	=	wave number of the sinusoidal wave
M_a	=	acoustic Mach number, ratio of particle velocity, and small-signal speed of sound
m	=	parameter for plane, cylindrical, and spherical waves
Pr	=	Prandtl number
p	=	acoustic pressure fluctuation
p_o	=	initial pressure amplitude of the sinusoidal wave
$\tilde{p}(r,\omega)$	=	complex Fourier transform of pressure with respect to retarded time
Q	=	amplitude of complex Fourier transform of square of pressure
q	=	square of the acoustic pressure fluctuations
$\tilde{q}(r,\omega)$	=	complex Fourier transform of square of pressure with respect to retarded time
r	=	range from the origin
r_o	=	source radius
t	=	time
y_s	=	distance between source and observer
y_I	=	distance between image and observer
α	=	real part of α' representing atmospheric absorption (neper/m)
α'	=	complex atmospheric absorption and dissipation coefficient
β	=	coefficient of nonlinearity
β_d	=	complex part of α' representing dissipation (1/m)
γ	=	ratio of specific heats
Δy	=	absolute difference in the distance of source and image from the observer
Δt	=	time lag between the arrival of sound from the source and the reflected sound
δ	=	thermoviscous coefficient
δt	=	time step for data sampling
ε	=	nonlinear coefficient
ν	=	coefficient of viscosity
ρ	=	ambient density
τ	=	retarded time
ϕ	=	phase of complex Fourier transform of pressure
ψ	=	phase of complex Fourier transform of square of pressure
ω	=	angular frequency (rad/s)

Presented as Paper 2934 at the 14th AIAA/CEAS Aeroacoustics Conference, Vancouver, British Columbia, Canada, 5–7 May 2008; received 17 April 2008; revision received 12 September 2008; accepted for publication 13 September 2008.

*Graduate Student, Department of Aerospace Engineering, 229 Hammond. Student Member AIAA.
†Boeing/A.D. Welliver Professor, Department of Aerospace Engineering, 223C Hammond. Fellow AIAA.
‡Boeing Technical Fellow, Post Office Box 3707. Associate Fellow AIAA.

I. Introduction

THE jet noise generated by modern jet fighter aircraft is sufficiently loud that its propagation to a distant observer is not linear but involves a steepening of the wave fronts and shock coalescence: the propagation is nonlinear. In addition, the character of the sound is very different from the usual rumble of jet noise, and the jet is said to "crackle." Previous methods to predict the nonlinear propagation of broadband jet noise have used either the Burgers equation [1] or the one-dimensional Navier–Stokes equations [2]. In the latter case, the Navier–Stokes equations were augmented to account for atmospheric absorption effects. An explicit analytical solution to the Burgers equation is available only for cases without atmospheric absorption. The Cole–Hopf transformation converts the nonlinear Burgers equation to a linear diffusion equation for

sinusoidal waves, which can be solved analytically. Previous numerical solutions based on the Burgers equation have used a split-step method, where the nonlinear steepening is predicted in the time domain from the Earnshaw solution [3], and the atmospheric absorption effects are predicted in the frequency domain. Though results using this approach, such as those by Gee [4], have shown promising agreement with available measurements, the technique involves resampling the time history at every time step, because the Earnshaw solution does not give the waveform at equal time spacing. This problem is avoided in the present approach. Brouwer [5] described a nonlinear propagation algorithm based on a solution of the generalized Burgers equation (GBE) with some similarities to the present approach. However, his formulation involved the solution of a system of coupled ordinary differential equations for the complex Fourier components of the pressure. The required summations for the nonlinear terms are not required in the present approach. The results obtained for the propagation of a pure tone are similar to those obtained with the present approach, described later. However, he approximated the broadband noise source spectrum with a weighted white noise spectrum. In addition, in the present calculations, the measured time histories of the source are used.

During takeoff or landing of an aircraft or during ground testing, the ground surface acts as a reflector for the pressure waves. The ground reflection is a correction of the sphericity of the wave front. Previously, Rao et al. [6], Ingard [7], and Salomons [8] performed experiments and analyses to study the effects of ground reflection on noise propagation. The full-scale military jet engine tests performed by Gee et al. [9,10] near the ground show the ground effects in the data. Attenborough [11] has given a review of ground effects in outdoor sound propagation.

In the present paper, a new algorithm is introduced in which both the nonlinear and atmospheric effects are predicted in the frequency domain. This avoids the need for resampling and preserves some of the statistical properties of the waveform that appear to be lost during the resampling process.

The GBE [12] is solved with the combined effects of nonlinearity and losses due to atmospheric absorption. The equation can be used for both plane and spreading waves. The propagation of a plane sinusoidal waveform, for which analytic solutions exist, is used as a benchmark problem to validate the method. The Fubini, Blackstock Bridging Function, and Fay analytical solutions [1] for sinusoidal waves are used for the validation. Next, comparisons are made with heated subsonic and supersonic broadband jet noise data generated in the Boeing Low Speed Aeroacoustic Facility [13]. The method is also used to propagate full-scale supersonic F/A-18E engine data [9] for large distances. Finally, the effect of ground reflections, which is an issue of importance when tie-down testing of aircraft engine noise is performed, is examined, both for the Boeing and the full-scale F/A-18E data.

II. General Analysis and Numerical Method

A nonlinear second-order wave equation derived from the mass, momentum, and energy conservation equations can be written in different forms, useful for different purposes. The nonlinear wave equation can be written for planar lossless waves, and plane and general 3-D waves with losses or diffraction [1]. The nonlinear wave equation for plane progressive waves is called the Westervelt equation [12], where cumulative nonlinear effects dominate local nonlinear effects. The equation can be simplified to describe the combined effects of nonlinearity and losses to form a generalized Burgers equation [1], which can be further simplified for plane waves. Another modification is known as the KZK (Khokhlov-Zabolotskaya-Kuznetsov) equation [1], which accounts for the combined effects of diffraction, absorption, and nonlinearity in directional sound beams. The Burgers equation is the simplest model that describes the combined effects of nonlinearity and losses. The generalized Burgers equation, which can model noise propagation for acoustic waves in the atmosphere with nonlinear and absorption effects, is used in the current approach.

Consider progressive waves in a compressible fluid. The form of Burgers equation for the pressure signal as a function of range r and retarded time τ is given by Morfey and Howell [14] as

$$\frac{\partial p}{\partial r} + m\frac{p}{r} - \frac{\varepsilon}{2}\frac{\partial p^2}{\partial \tau} = \frac{\delta}{2}\frac{\partial^2 p}{\partial \tau^2} \tag{1}$$

The parameter m is equal to 0, 1/2, and 1 for plane, cylindrical, and spherical waves, respectively. The square of the pressure $p^2(r,\tau)$ will be written as $q(r,\tau)$ in Eq. (1). The thermoviscous coefficient δ in Eq. (1) is given by

$$\delta = \left(\frac{\nu}{c_o^3}\right)\left(\frac{4}{3} + \frac{\gamma - 1}{Pr}\right) \tag{2}$$

The nonlinear coefficient ε in Eq. (1) is given by $\varepsilon = \beta/\rho c^3$. The value of β is given by $(\gamma+1)/2$ for perfect gases and by $1 + B/2A$ for arbitrary fluids where it can hold positive, zero, and negative values. $B/2A$ is the coefficient of the first nonlinear term in an assumed pressure-density relation. The square of the pressure signal $q(r,\tau)$, has the frequency range that is twice that of the pressure signal. Hence, the pressure time waveform is interpolated to double the sample rate, and the interpolated signal is used to calculate $q(r,\tau)$. The complex Fourier transform of Eq. (1) taken with respect to τ gives

$$\frac{\mathrm{d}\tilde{p}}{\mathrm{d}r} + m\frac{\tilde{p}}{r} + \alpha'\tilde{p} = \frac{i\omega\varepsilon}{2}\tilde{q} \tag{3}$$

where $\alpha' = \alpha + i\beta_d = \omega^2\delta/2$. The atmosphere is assumed to be homogenous and at rest. The atmospheric absorption and dispersion losses are calculated using the O_2 and N_2 relaxation frequencies by the method described by Bass et al. [15,16]. The complete formulation for α' is given by

$$\alpha'(f) = (\alpha_{\mathrm{tvb}} + \alpha_{\mathrm{rN}} + \alpha_{\mathrm{rO}}) - i\left(\frac{\alpha_{\mathrm{rN}}}{f_{\mathrm{rN}}} + \frac{\alpha_{\mathrm{rO}}}{f_{\mathrm{rO}}}\right)f \tag{4}$$

where α represents the absorption coefficient due to a given process denoted by the subscripts tvb, rN, and rO, which signify thermoviscous/bulk, relaxation of nitrogen, and relaxation of oxygen, respectively. Similarly, β_d is given by the complex part of Eq. (4) where f_{rN}, and f_{rO} denote the relaxation frequencies of nitrogen and oxygen, respectively. The absorption coefficient components and relaxation frequencies in Eq. (4) can be calculated according to the formulas given by Bass et al. The Fourier transforms of $p(r,\tau)$ and $q(r,\tau)$ are given by

$$\tilde{p}(r,\omega) = \frac{1}{2\pi}\int_{-\infty}^{\infty} p(r,\tau)e^{-i\omega\tau}\,\mathrm{d}\tau \tag{5a}$$

and

$$\tilde{q}(r,\omega) = \frac{1}{2\pi}\int_{-\infty}^{\infty} p^2(r,\tau)e^{-i\omega\tau}\,\mathrm{d}\tau \tag{5b}$$

where a tilde denotes the complex Fourier transform. The complex Fourier transforms of $p(r,\tau)$ and $q(r,\tau)$ can be written in terms of their amplitude and phase as

$$\tilde{p}(r,\omega) = A(r,\omega)e^{i\phi(r,\omega)} \tag{6a}$$

and

$$\tilde{q}(r,\omega) = Q(r,\omega)e^{i\psi(r,\omega)} \tag{6b}$$

The amplitude and phase are given by

$$A(r,\omega) = (\tilde{p}\tilde{p}^*)^{1/2} \tag{7a}$$

$$\phi(r,\omega) = \arctan[\tilde{p}_{\mathrm{Im}}/\tilde{p}_{\mathrm{Re}}] \tag{7b}$$

where the asterisk denotes a complex conjugate, the subscript Im represents the imaginary part, and the subscript Re the real part of

$\tilde{p}(r,\omega)$ or $\tilde{q}(r,\omega)$. The values of $\tilde{p}(r,\omega)$ and $\tilde{q}(r,\omega)$ from Eqs. (6a) and (6b) are replaced in Eq. (3) to obtain the following differential equation:

$$\left(iA\frac{\mathrm{d}\phi}{\mathrm{d}r}+\frac{\mathrm{d}A}{\mathrm{d}r}\right)e^{i\phi}+\frac{Ae^{i\phi}}{r}-\alpha' Ae^{i\phi}=\frac{i\omega\varepsilon}{2}Qe^{i\psi} \tag{8}$$

The real and imaginary components of Eq. (8) can be used to obtain differential equations for the evolution of the amplitude and phase of the Fourier transform of the pressure. These equations take the form

$$\frac{\mathrm{d}A}{\mathrm{d}r}=-\frac{A}{r}-\frac{\omega\varepsilon Q}{2}\sin(\psi-\phi)-\alpha A \tag{9a}$$

and

$$\frac{\mathrm{d}\phi}{\mathrm{d}r}=\frac{\omega\varepsilon}{2}\frac{Q}{A}\cos(\psi-\phi)-\beta_d \tag{9b}$$

These equations are solved using a second-order Runge–Kutta finite difference scheme to find the amplitude $A(r+\delta r,\omega)$ and phase $\phi(r+\delta r,\omega)$ of the pressure in the frequency domain at the next range step. The complex pressure is converted back to the time domain using the inverse Fourier transform before moving to the next step. The square of the pressure signal is again calculated from the interpolated pressure signal. The whole process is then repeated. If the required distance is reached, the inverse Fourier transform is the last step required to obtain the solution in the time domain. This approach will be called the nonlinear frequency-domain algorithm (NLFDA).

It should be noted that the present algorithm automatically constructs the ordinary differential equations for the amplitude and phase of the frequency components by finding the Fourier transform of the square of the pressure. This avoids the need to construct the series representation of the nonlinear terms as proposed by Brouwer [5]. In addition, there is no requirement to resample the predicted waveform at each range step, as in Gee [4], as the pressure time history is always determined at a constant sampling rate.

In addition to nonlinear propagation into free space, the present study includes the effect of reflections from a ground plane. This is important in situations such as the tie-down testing of full-scale engines. For simplicity, the ground is treated as rigid and perfectly reflecting. The geometry for the ground reflection study is shown in Fig. 1.

The symbols in the Fig. 1 are self-explanatory. There is a time lag between the arrival of sound from the source and the reflected sound because the distance traveled by the reflected wave is greater than the distance traveled by the wave coming directly from the source. This time difference Δt is given by

$$\Delta t=\Delta y/c \tag{10}$$

where $\Delta y=|y_I-y_s|$ and y_I and y_s can be calculated from Fig. 1 by

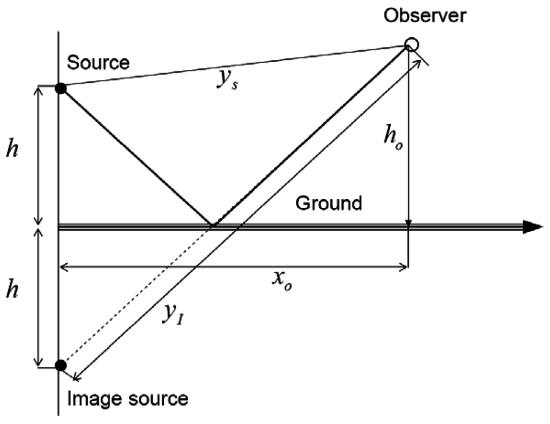

Fig. 1 Geometry used for the ground reflection study.

$$y_s=\sqrt{x_o^2+(h_o-h)^2};\qquad y_I=\sqrt{x_o^2+(h_o+h)^2} \tag{11}$$

The total number of data points to be shifted for the sound received from the image is given by

$$N_{\text{shift}}=\Delta t/\delta t \tag{12}$$

where δt is the data sampling time-step size. The pressure waveforms thus obtained from the source and image are superimposed to obtain the total sound at the observer.

III. Results and Discussions

Three cases, as already stated, are considered for the evaluation of the NLFDA developed to solve the Burgers equation. The predicted linear and nonlinear results for all the cases are compared with the experimental measurements. The ground reflection formulation presented in the previous section is then used to study these effects on both the Boeing LSAF and F/A-18E data.

A. Sinusoidal Wave

In this section, a sinusoidal plane progressive wave is propagated and the results are compared with the analytical solutions. The shock formation distance for a plane sinusoidal wave is given by

$$\bar{x}=\frac{1}{\beta M_a k} \tag{13}$$

where the wave number k is equal to $2\pi f/c$. A dimensionless parameter $\sigma=x/\bar{x}$ is used to define the propagation distance in the preshock and the postshock regions for the plane sinusoidal wave. The shock formation distance for the sine wave corresponds to $\sigma=1$.

The pressure waveform and power spectral density (PSD) are computed at different values of σ. The benchmark analytical results for the initially sinusoidal waveform include the Fubini solution ($0<\sigma<1$), the Fay solution ($\sigma>3$), and the Blackstock Bridging Function (BBF) [1]. The BBF bridges the gap between the Fay and Fubini solutions by taking into account the second root of the transcendental function obtained while solving the wave equation for sine waves. However, it should be noted that only the Fay solution includes atmospheric absorption effects. The initial pressure waveform is given by

$$p(r,t)=p_o\sin(2\pi f_o t) \tag{14}$$

The present method is applied to this signal, and the time waveform and the PSD are obtained at different values of σ.

A test case of a sinusoidal wave with pressure amplitude $p_o=$ 140 dB re 20 μPa and fundamental frequency $f_o=1000$ Hz is considered. The sampling rate is 64 kHz and 2000 cycles are used for propagation. Sets of 1024 points are averaged with 50% overlap to calculate the PSD values. Sixty harmonics are used to obtain the waveform for all the solutions.

The predicted and analytical Fubini time waveform and PSD plots are shown in Figs. 2 and 3, respectively, for $\sigma=0.95$. This is just before the shock formation distance is reached. The predicted and analytical results show excellent agreement. Similar comparison plots are presented in Figs. 4 and 5 for $\sigma=3.0$ with the BBF. The predicted time waveform for $\sigma=3.0$ has a few spikes because of the wave steepening after the shock formation. Also, the amplitude of the predicted waveform is slightly higher than the analytical solution. This could be corrected with the addition of a low-pass filter. Good agreement is illustrated between the predicted harmonic values and the BBF results in the PSD plots. However, the amplitude of the NLFDA predictions is slightly higher than the analytical solution. As shown in Eq. (14), the initial waveform contained only the fundamental frequency f_o. The generation of harmonics shown in the PSD plots is due to the nonlinear effects where the harmonics grow at the expense of the energy of the fundamental tone.

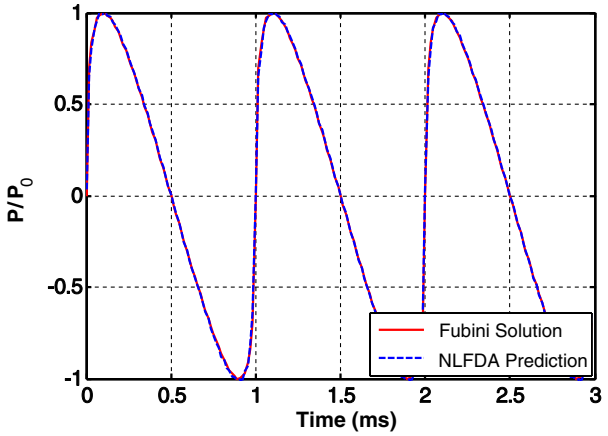

Fig. 2 NLFDA prediction and Fubini analytical time waveform at $\sigma = 0.95$ ($f_o = 1000$ Hz, $\mathrm{SPL}_o = 140$ dB re 20 μPa).

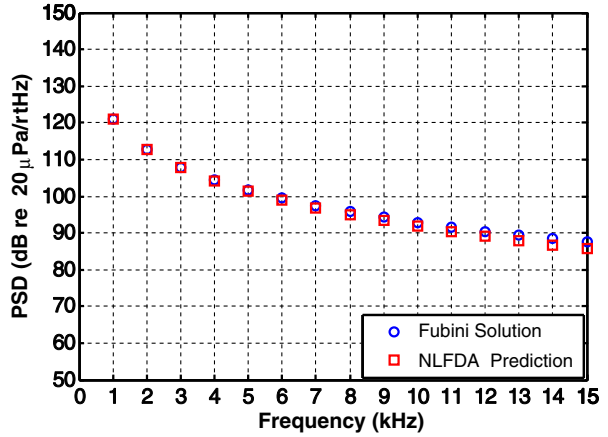

Fig. 3 NLFDA prediction and Fubini analytical PSD plot at $\sigma = 0.95$ ($f_o = 1000$ Hz, $\mathrm{SPL}_o = 140$ dB re 20 μPa).

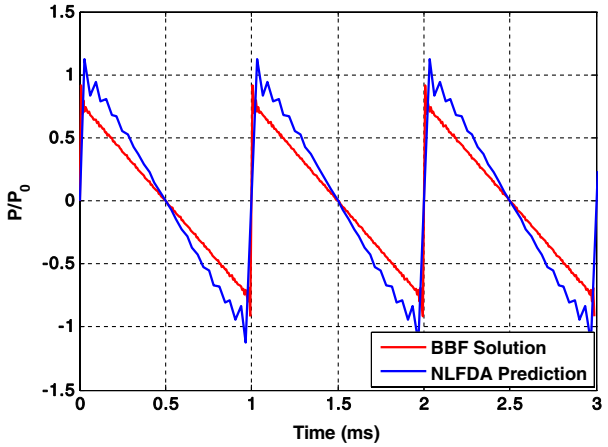

Fig. 4 NLFDA prediction and BBF time waveform at $\sigma = 3.0$ ($f_o = 1000$ Hz, $\mathrm{SPL}_o = 140$ dB re 20 μPa).

B. Broadband Data from the Boeing Low Speed Aeroacoustic Facility

In addition to the sinusoidal case, for which an analytical solution exists, broadband jet noise source data obtained in the Boeing LSAF are used to assess the NLFDA prediction methodology. The phenomenon of nonlinear propagation is more prevalent than is commonly recognized. Viswanathan [17] first reported the observation of this phenomenon for heated subsonic laboratory jets and identified the convective Mach number as a reliable indicator for predicting the onset of nonlinear effects. Specifically, when the convective Mach number exceeds unity, there is transfer of energy to the higher frequencies, manifested by increased spectral levels. This agglomeration is independent of the overall sound amplitude and is controlled mainly by the convective Mach number (see [13,18] for further details). For the sake of completeness, the following overview of the experimental measurements is provided.

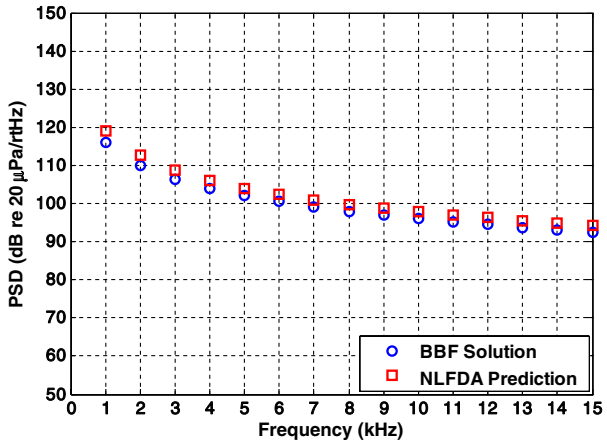

Fig. 5 NLFDA prediction and BBF analytical PSD plot at $\sigma = 3.0$ ($f_o = 1000$ Hz, $\mathrm{SPL}_o = 140$ dB re 20 μPa).

Four microphones at four different physical distances of 10.59 ft (3.23 m), 16.59 ft (5.06 m), 22.59 ft (6.89 m), and 30.59 ft (9.33 m) from the nozzle exit plane and at a polar angle of 150 deg were installed. These pole-mounted microphones were located at different azimuthal angles so as to eliminate the interference due to the poles, etc. Free-field time-series data in a controlled environment inside an anechoic chamber were acquired for a variety of jet operating conditions. The data were sampled at 192 kHz. A convergent nozzle with a diameter of 2.45 in. (6.22 cm) and a convergent–divergent nozzle with an exit diameter of 1.25 in. (3.18 cm) and a design Mach number of 1.9 were used in the test. The nondimensional microphone distances (r/D) for the two nozzles are 52, 81, 111, and 150 for the convergent nozzle and 100, 157, 213, and 289 for the convergent–divergent nozzle, respectively. A sample result, Fig. 10 from [13], is included as Fig. 6 here, to provide context and clearly illustrate the effects of nonlinear propagation. The normalized spectra from the four microphones, assuming linear propagation, have been corrected to a common distance of 20 ft (6.1 m) from an unheated and a highly heated jet at a Mach number of 0.9 in Fig. 6. The ratio of the static temperature at the jet exit and the ambient temperature $TR = 2.84$ for the heated jet. There is very good collapse of the spectra for the unheated jet. However, the spectral levels at the high frequencies progressively increase as the propagation distance is increased for the highly heated jet. The current method aims to predict this nonlinear effect with transfer of energy to the higher frequencies.

Two test cases, a heated subsonic jet with $M = 0.9$ and $TR = 2.84$, and a supersonic heated jet with $M = 1.9$ and $TR = 1.65$, have been considered. The pressure signal for the subsonic case is propagated from the initial measurement location of 52 D_j (jet exit diameter) from the jet exit. The initial overall sound pressure level (OASPL) is 127.3 dB re 20 μPa. Figures 7–9 show the linearly and nonlinearly predicted and experimental PSD. The linear predictions are obtained by omitting the nonlinear term from the Burgers equation. It can be seen from Fig. 7 that the PSD levels are higher as compared to linear predictions at frequencies above 30 kHz. These high values show the onset of nonlinearity in the propagation. The nonlinear prediction code captures this nonlinear effect and shows the rise in the PSD levels at high frequencies. The nonlinear effects cumulate over distance, thus giving more high-frequency lift in the PSD levels at 111 D_j and 150 D_j shown in Figs. 8 and 9, respectively. The linear predictions cannot capture this lift and deviate further from the experimental and nonlinear results at larger distances.

For the supersonic case, the pressure signal is propagated from the initial measurement location of 100 D_j from the jet exit. The initial OASPL of the pressure signal at 100 D_j is 131 dB re 20 μPa.

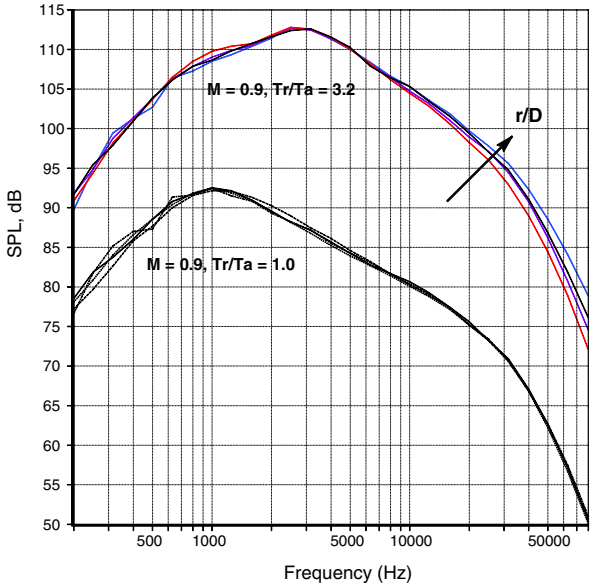

Fig. 6 Data normalized to 20 ft and standard day conditions from measurements at different microphone distances (angle = 150 deg, $M = 0.9$, $Tt/Ta = 1.0$ and 3.2). Upper curves: $r = 10.59$, 16.59, 22.59, and 30.59 ft. The trend with increasing microphone distance is shown in the figure.

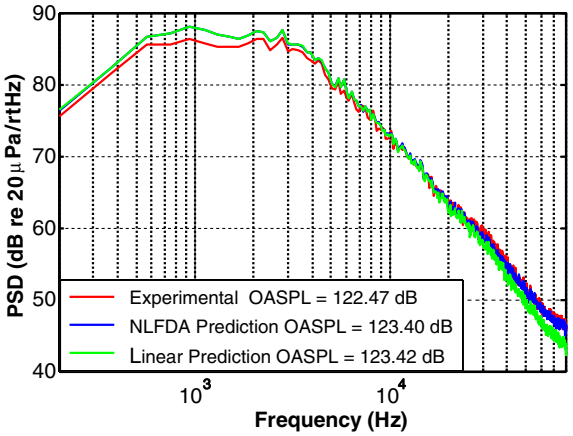

Fig. 7 Experimental results and linear and nonlinear predictions for LSAF subsonic data at 81 D_j ($M = 0.9$, $TR = 2.84$).

Figure 10 shows a comparison between the linear and nonlinear predicted and experimental results at 157 D_j from the jet exit. The nonlinear effects transfer energy to the high frequencies, manifested as a rise in the PSD levels compared to linear propagation. The predicted spectrum captures the lift at high frequencies owing to nonlinear wave steepening. The data are propagated further to 213 D_j, shown in Fig. 11, and reasonable agreement is observed between the predicted and experimental results. Figure 12 shows the propagated data at 289 D_j. It can be observed that the linear results are not able to capture the rise at high frequencies. These results also match well with the predictions by Gee [4] for the same LSAF data. The OASPL also agree fairly well for the experimental, the linear, and the nonlinear results for all distances from the jet exit.

The skewness for both the test cases has been calculated for the experimental and predicted results. The results are tabulated for the subsonic heated case in Table 1 and for the supersonic heated case in Table 2. The predicted skewness values in Table 1 show good agreement with the experimental values at all distances. The skewness of the signal decreases with distance. Table 2 shows a similar trend for the change of skewness for the predictions as in Table 1, but the experimental skewness increases with distance. It should be noted that the measurement angle of 150 deg is in the peak

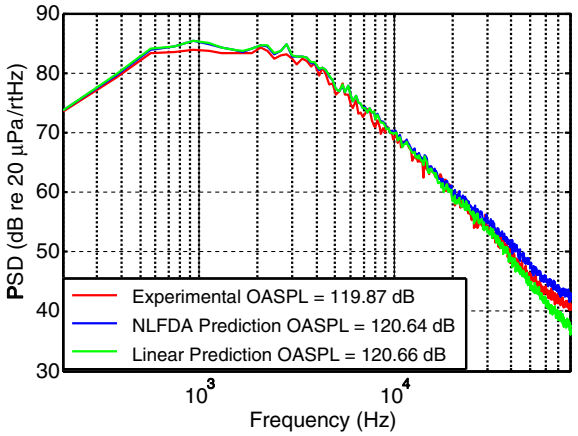

Fig. 8 Experimental results and linear and nonlinear predictions for LSAF subsonic data at 111 D_j ($M = 0.9$, $TR = 2.84$).

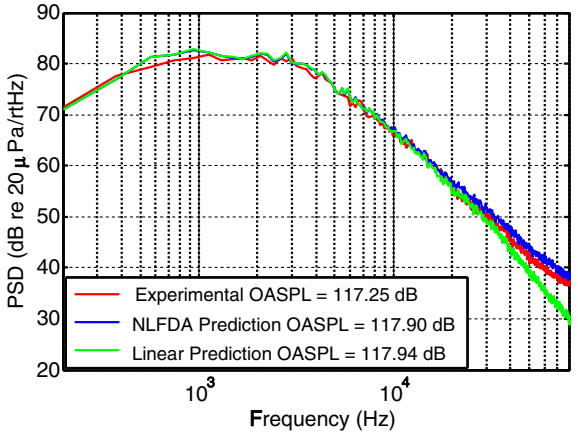

Fig. 9 Experimental results and linear and nonlinear predictions for LSAF subsonic data at 150 D_j ($M = 0.9$, $TR = 2.84$).

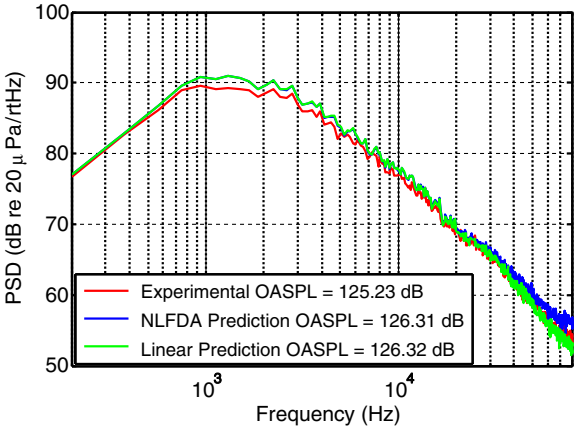

Fig. 10 Experimental results and linear and nonlinear predictions for LSAF supersonic data at 157 D_j ($M = 1.9$, $TR = 1.65$).

noise direction for the subsonic case, but is not in the peak noise direction for the supersonic case. The reason for this discrepancy between the data and the predictions is not clear. The number of zero crossings for the Boeing LSAF data, over the sample length of 0.41 s, is given as a function of distance from the nozzle exit in Table 3. The number of zero crossings decreases with distance, both in the experimental and predicted results.

Recent experimental observations, such as those presented by Gee et al. [19], suggest that the peak frequency in the measured spectrum shifts to lower frequencies with increasing nonlinear propagation

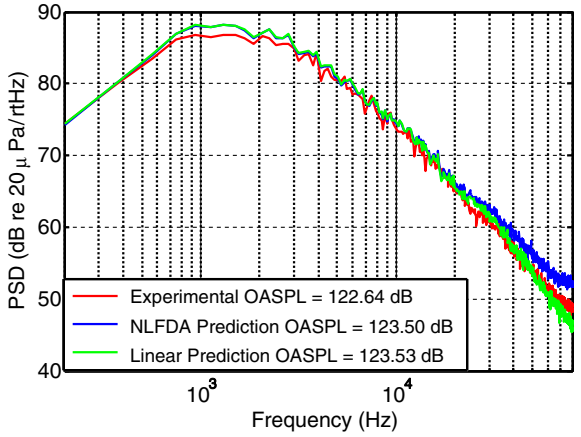

Fig. 11 Experimental results and linear and nonlinear predictions for LSAF supersonic data at 213 D_j ($M = 1.9$, $TR = 1.65$).

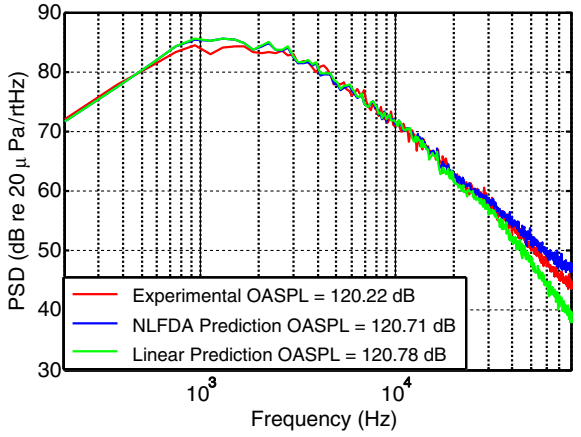

Fig. 12 Experimental results and linear and nonlinear predictions for LSAF supersonic data at 289 D_j ($M = 1.9$, $TR = 1.65$).

distance. An explanation offered for this phenomenon is that there is shock coalescence, which reduces the number of zero crossings and hence increases the levels at low frequencies. As shown in Table 3 of the present paper, there is a decrease in the number of zero crossings with distance, but this does not result in a shift of the spectral peak. There is a good explanation, which has nothing to do with zero crossings, for the observed shift in the peak to the lower frequencies with increasing distance. It is well established from a variety of source measurements that the sources of jet noise extend over several jet diameters and that the low-frequency sources are located farther downstream than high-frequency sources. A compilation of the source locations for subsonic jets by Fisher et al. [20] indicated that the centroids for Strouhal numbers less than 0.1 lies beyond 12 jet diameters (see Fig. 9 in [20]). For a supersonic jet, the length of the potential core is much longer than for subsonic jets, and the low-frequency sources extend to ~2 potential core lengths. Recent source location data for a $M = 1.9$ jet presented by Viswanathan [21] show that the peak source region for a Strouhal number of 0.13 extends from ~10 D_j to ~25 D_j and that the peak location for the overall sound pressure level is at ~15 D_j.

Consider the experimental setup of [19]. The microphone array is centered at 4 D_j, with the closest microphone at 10 jet diameters. With simple trigonometry, it is easy to verify that the microphone located at 10 D_j is actually in the upstream direction from the centroid of the low-frequency source, which is taken to be at 15 D_j. It is also apparent that, as the distance of the microphone increases, the discrepancy between the actual radiation angle and the assumed angle of 145 deg from the origin at 4 D_j keeps decreasing. The radiation angles for the farthest two microphones are nearly equal. Therefore, nearly identical spectral shapes are observed for these two microphones. The measured spectra in the near field have different shapes, being at different radiation angles for the distributed sources. It is not surprising then that the measured spectra in the near field have different peak frequencies than those at larger distances. Therefore, the observed shift in peak frequency is a consequence of the measurements being in the near field and is not connected to the reduction in zero crossings as suggested in [19].

Now, why is no shift in peak frequency observed in the Boeing data? For the subsonic jets, the closest microphone is at 52 D_j. As shown in Fig. 6, the assumption of a point source located at the nozzle exit in the scaling of the data to a common distance leads to good collapse of the spectra from the four microphones; that is, the closest microphone is located in the true far field. The wiggles seen at the lower frequencies in one of the spectra are due to reflections from the exhaust collector, as explained in Viswanathan [13,22]. The $M = 1.9$ jet has a more extended source region; the closest microphone is at 100 D_j. As shown in Fig. 9 in [13], the normalized spectra from the four microphones show very good collapse at the lower frequencies for this supersonic jet as well. Once again, the nearest microphone is in the true far field. It should be clear that the data used for the assessment of the NLFDA in the present paper all had initial distances sufficiently large that the measurements are in the true far field and that the angle difference due to the distributed sources is small, even for the low frequencies. Thus, the directivity of the source does not influence the nonlinear propagation predictions. It would be desirable to include the distributed nature of the sources in the method for the nonlinear propagation of broadband jet noise; however, this problem is not significant if the initial measurement location is already in the far field for the distributed sources.

C. Full-Scale F/A-18E Data

The F/A-18E [9] run-up measurements were conducted at the U.S. Naval Air Engineering Station, Lakehurst, New Jersey in April 2003. Recordings were made with both engines idling (Idle), at military thrust (Mil), and with afterburners engaged (AB). The ambient temperature and the relative humidity were 20°C and 50%, respectively, and average wind speeds were approximately 3 m/s at a height of 4.5 m. The microphone measurements were taken at 18, 74, and 150 m from the engine nozzles along a radial line 135 deg from the forward direction, which is approximately the peak noise direction for the F/A-18E at high-thrust conditions. The 18 m data set was acquired with a 6.35 mm Bruel and Kjaer 4938 condenser microphone flush-mounted in an aluminum plate baffle located horizontally on the pavement. The 74 and 150 m data were acquired

Table 1 Skewness values for NLFDA predicted and experimental data for LSAF heated subsonic data ($M = 0.9$, $TR = 2.84$)

	$R/D_j = 81$	$R/D_j = 111$	$R/D_j = 150$
Experimental skewness	0.247	0.209	0.190
NLFDA predicted skewness	0.211	0.199	0.184

Table 2 Skewness values for NLFDA predicted and experimental data for LSAF heated supersonic data ($M = 1.9$, $TR = 1.65$)

	$R/D_j = 157$	$R/D_j = 213$	$R/D_j = 289$
Experimental skewness	0.164	0.176	0.216
NLFDA predicted skewness	0.183	0.156	0.128

Table 3 Number of zero crossings for NLFDA predicted and experimental data for LSAF heated supersonic data ($M = 1.9$, $TR = 1.65$)

	$R/D_j = 157$	$R/D_j = 213$	$R/D_j = 289$
Experimental number	5090	4518	4268
NLFDA predicted number	5138	4744	4300

with handheld Endevco 8510C-15 piezoresistive pressure transducers located about 1.2 m above grassy ground. All data were recorded with portable Sony TCD-D8 digital audio tape recorders sampling at 44.1 kHz.

The measurements shown in Fig. 13 are taken at 18 m and propagated to 74 and 150 m using the linear and nonlinear algorithm. The measurements at 74 and 150 m were made close to the ground, which affects the signal due to ground reflection and atmospheric refraction.

The OASPL for AB at 18 m is 151 dB. Figures 14 and 15 show the predicted PSD of the propagated signal at 74 and 150 m, respectively. The decrease in the PSD slope at high frequencies between the linear and nonlinear predictions can be seen by comparing Figs. 14 and 15. The rise in the PSD levels at high frequencies can also be seen in these plots. The linear predictions are shown for a comparison.

The propagation distances in Figs. 14 and 15 are long enough to cause sufficient cumulative nonlinearity, as well as high counteracting atmospheric absorption, as evident in the linear predictions. Because of these effects, there is approximately 40 dB difference in the predicted nonlinear and linear results at 74 m, which increases further to 80 dB at 150 m for a frequency of 20 kHz. Therefore, nonlinearities make a significant difference in this case. In Figs. 14 and 15, there is a rapid increase in the predicted levels above 20 kHz. This was also noticed by Brouwer [5] who suggested that this increase was a numerical error in his simulations. The present results were recalculated with twice the frequency resolution by interpolating the time history with half the time step. There was no change in the rise above 20 kHz. It should also be noted that there is no such rapid increase in the comparisons with the Boeing model scale data. Therefore, the rapid rise is not thought to be associated with a numerical error. It is possible that there are measurement errors in the phase of the signal measured at 18 m. However, no complete explanation of this observation is available at this time.

Unfortunately, the authors were unable to obtain the experimental data for comparisons. However, as shown by Gee et al. [9], the experimental data are strongly affected by ground reflections. This is considered in the next section.

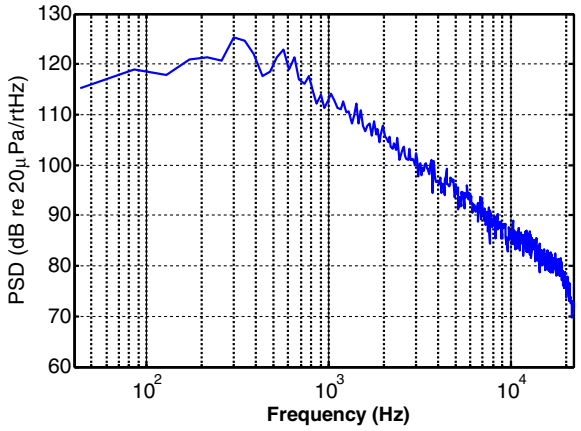

Fig. 13 PSD plot at 18 m for the experimental data of F/A-18E.

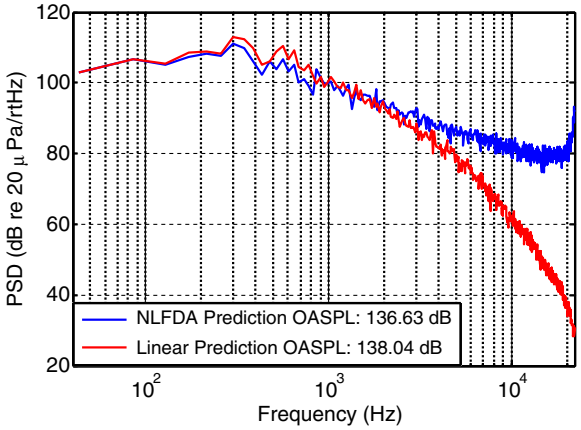

Fig. 14 Linear and nonlinear predicted results at 74 m from jet exit for supersonic full-scale F/A-18E engine.

D. Ground Reflection

Two cases are considered to study ground reflection effects. The first case is the Boeing LSAF supersonic data set, and the second case is the full-scale F/A-18E experimental data set, both used in an earlier section to study nonlinear effects. The model explained in the numerical method section is used to study the ground effects. The NLFDA is used to propagate the signal from both the real and image sources. In the present, simple formulation, it is assumed that the source and its image are perfectly coherent and that the source has perfect spherical symmetry and correlation. It is expected that the actual jet noise source would not satisfy these conditions. However, the present calculations are used to demonstrate the qualitative effects of ground reflection. These are shown to be consistent with the experimental observations in the full-scale experiment.

1. *Boeing Low Speed Aeroacoustic Facility Supersonic Data Set*

The Boeing supersonic heated jet case ($M = 1.9$, $TR = 1.65$) is taken first to study the effects of ground reflection by varying the observer height from an assumed ground. The data are propagated from 100 to 157 D_j using the NLFDA, and the ground reflection formulation is used to obtain PSD levels from the interaction of the

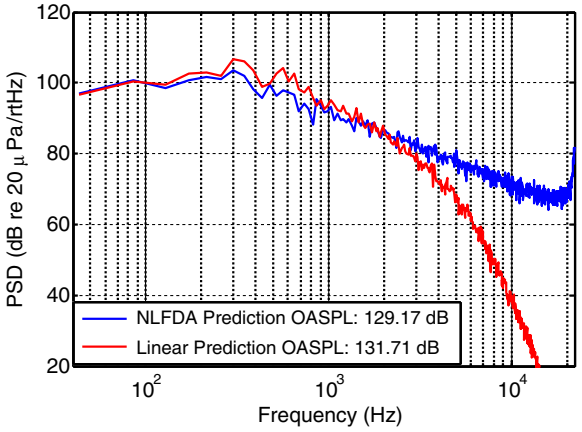

Fig. 15 Linear and nonlinear predicted results at 150 m from jet exit for supersonic full-scale F/A-18E engine.

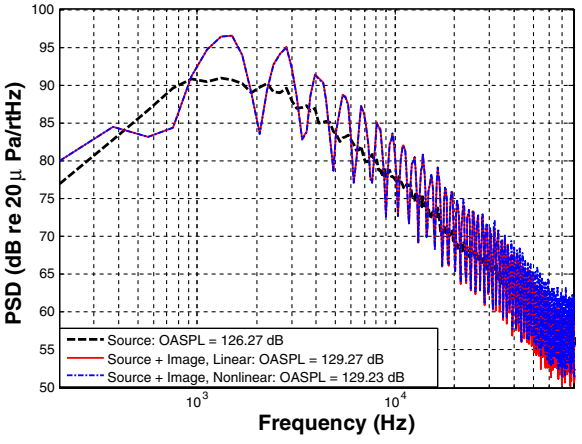

Fig. 16 Ground effects calculated using NLFDA and linear propagation at 157 D_j for Boeing LSAF data, observer at 25 in. from ground ($M = 1.9$, $TR = 1.65$).

incident and reflected waves from an assumed rigid ground. Figure 16 shows the PSD levels before and after considering the ground effects when the observer is at 0.64 m (25 in.) from the ground at 157 D_j from the jet exit. The linear results are also shown for comparison. The jet is placed at 0.38 m (15 in.) from the ground. It can be seen in this figure that the ground affects the PSD levels at frequencies as low as 1 kHz. The interference patterns can be seen in the PSD levels with a difference of approximately ± 6 dB between the maximum and minimum PSD levels. Also, the separations of the frequency of these peaks are about 1 kHz, as seen in the plot. The linear results match with the nonlinear results for all frequencies, except at frequencies above 30 kHz. Figure 17 shows the linear and nonlinear ground effects when the observer is at 0.89 m (35 in.) instead of 25 in. from the ground. It can be seen that the difference between the maxima and minima of the PSD levels is approximately 10 dB, which is less when compared with the previous case with an observer height of 25 in. The separation frequency of the maxima and minima is still about 1 kHz, though the first maximum occurs at a lower frequency as compared with the 25 in. case. Figure 18 shows the linear and nonlinear ground effects with the observer at 1.14 m (45 in.) from the ground. The difference between the maximum and minimum PSD level reduces further to 8 dB, and the first peak occurs at a lower frequency as compared with the previous cases with lower observer heights. There is no significant change in the frequency with which the maximum and minimum peaks occur.

Figure 19 compares the PSD levels with ground effects for the observer heights of 25, 35, and 45 in. in the same plot. It is clearly evident now that the peak frequency shifts to lower values with

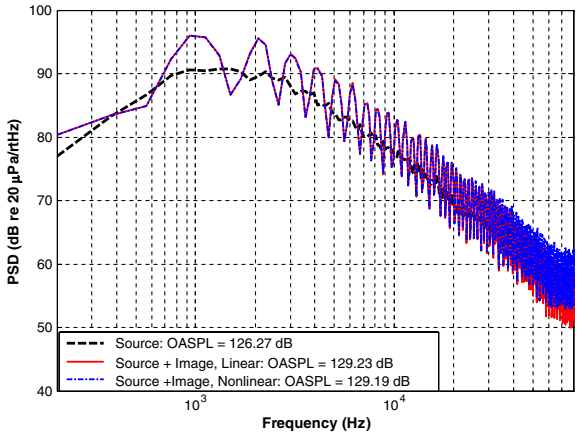

Fig. 17 Ground effects calculated using NLFDA and linear propagation at 157 D_j for Boeing LSAF data, observer at 35 in. from ground ($M = 1.9$, $TR = 1.65$).

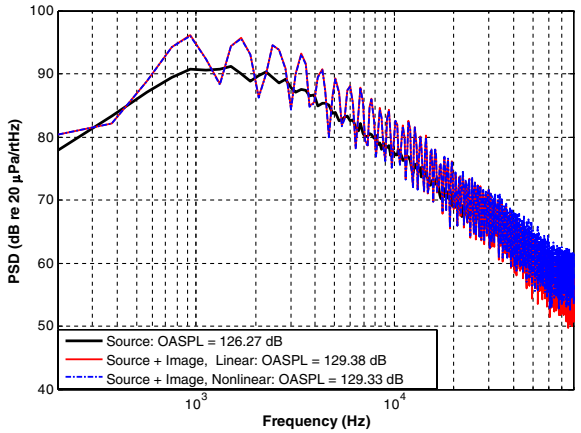

Fig. 18 Ground effects calculated using NLFDA and linear propagation at 157 D_j for Boeing LSAF data, observer at 45 in. from ground ($M = 1.9$, $TR = 1.65$).

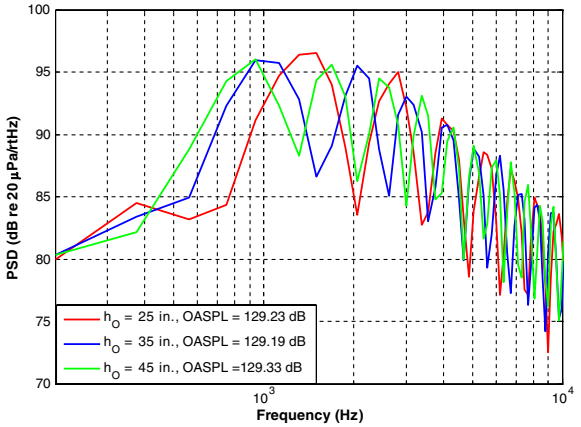

Fig. 19 Comparison of ground reflection results calculated using NLFDA at 157 D_j for Boeing LSAF data with observer at 25, 35, and 45 in. ($M = 1.9$, $TR = 1.65$).

increase in the observer height. By increasing the observer height from the ground, the path traveled by the reflected wave increases and thus more time delay is observed by the receiver. This reduces the frequency at which the constructive interference occurs for the first time. There is also less difference between the maximum and minimum PSD levels with increasing receiver height, as seen in the figure. There is an increase of approximately 3 dB in the OASPL after considering ground effects. However, the OASPL for the three different observer heights, when the ground reflections are included, are almost identical.

2. *Full-Scale F/A-18E Experimental Data Set*

Ground effects on the F/A-18E supersonic data are studied at different locations from the nozzle exit, while the nozzle and observer heights from the ground are kept fixed. Figures 20 and 21 show the predicted ground reflection effects at 74 and 150 m from the nozzle exit, respectively. The nozzle exit is assumed to be centered at 1.22 m (4 ft) and the receiver is at 1.52 m (5 ft) from the ground in all the cases. It can be observed from these figures that, as the distance from the nozzle exit becomes large as compared to the observer height, the constructive and destructive interference are observed only at higher frequencies in the PSD plots. This effect is due to the change in the phase difference for the two distances. The phase difference between the incident and reflected signal is caused both by the path length difference and by the phase change on reflection at the ground. For larger distances, as compared to the height of the observer from the ground, the path difference between the reflected and incident waves is decreased and the phase change is reduced. This causes the phase difference to increase at a slower rate with

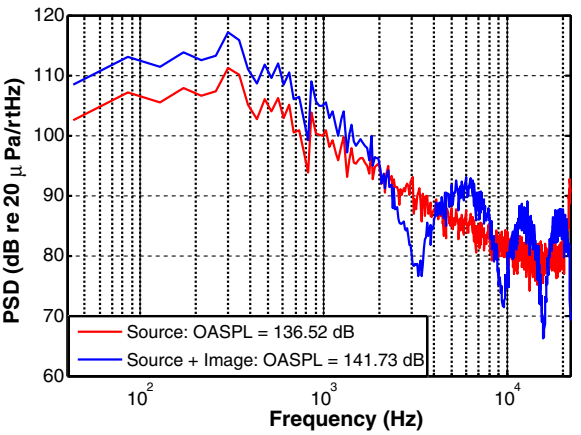

Fig. 20 Prediction results and ground reflection effects for a supersonic F/A-18E engine at 74 m from jet exit with source at 4 ft and receiver at 5 ft from the ground.

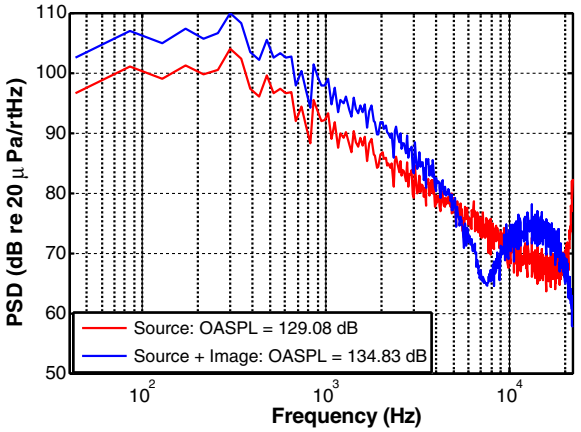

Fig. 21 Prediction results and ground reflection effects for a supersonic F/A-18E engine at 150 m from jet with source at 4 ft and receiver at 5 ft from the ground.

frequency. Thus, the minima and maxima are seen at larger frequency differences if the height of the observer is very small compared to its distance from the source.

Figure 20 shows the difference in the PSD values at 74 m with and without ground effects up to 2000 Hz. Figure 21 shows the difference in the PSD values at 150 m with and without ground effects up to 2000 Hz. Though the experimental data at these locations are not available to the authors, the results show qualitative agreement with the data shown by Gee et al. [9]. However, the terrain in those measurements was not a perfectly rigid, flat plane, and so exact agreement would not be expected.

IV. Conclusions

An algorithm for nonlinear noise propagation has been developed for solving the generalized Burgers equation in the frequency domain. The method can be applied to a monofrequency wave or a broadband signal with plane, cylindrical, or spherical spreading. The algorithm predicts the nonlinear behavior of jet noise propagation, including atmospheric absorption effects.

The results for a sinusoidal wave match well with the analytical Fubini and BBF solution. The method is then used to predict the nonlinear propagation of broadband jet noise. There is good agreement between the predictions and the Boeing LSAF data. The linear and nonlinear predicted results for the full-scale F/A-18E engine data show large differences at high frequencies. The effects of ground reflection have been demonstrated with the Boeing LSAF data as well as the F/A-18E data. The ground effects are observed only at high frequencies when the distance between the nozzle exit and observer is very large. The OASPL rises in the presence of a reflecting surface in all the cases. The nonlinear effects tend to grow with higher amplitudes of pressure fluctuations. At sufficiently high wave amplitudes and at larger distances, predictions based on the linear theory can show large deviations from the experimental data and the nonlinear predictions.

Acknowledgments

This work was supported by The Boeing Company. The authors would like to thank Boeing for providing Low Speed Aeroacoustic Facility data and the financial support for this project. The F/A-18E initial data was provided by Kent Gee.

References

[1] Blackstock, D. T., Hamilton, M. F., and Pierce, A. D., "Progressive Waves in Lossless and Lossy Fluids," *Nonlinear Acoustics*, edited by M. F. Hamilton, and D. T. Blackstock, 1st ed., Academic Press, San Diego, CA, 1998, pp. 68–71, 113–117.

[2] Wochner, M. S., Atchley, A. A., and Sparrow, V. W., "Numerical Simulation of Finite Amplitude Wave Propagation in Air Using a Realistic Atmospheric Absorption Model," *Journal of the Acoustical Society of America*, Vol. 118, No. 5, 2005, pp. 2891–2898. doi:10.1121/1.2047109

[3] Hamilton, M. F., and Morfey, C. L., "Model Equations," *Nonlinear Acoustics*, edited by M. F. Hamilton and D. T. Blackstock, 1st ed., Academic Press, San Diego, CA, 1998, pp. 41–62.

[4] Gee, K. L., "Prediction of Nonlinear Jet Noise Propagation," Ph.D. Dissertation, Graduate Program in Acoustics, Pennsylvania State Univ., University Park, PA, 2005.

[5] Brouwer, H. H., "Numerical Simulation of Nonlinear Jet Noise Propagation," *14th AIAA/CEAS Aeroacoustics Conference*, AIAA Paper 2005-3088, May 2005.

[6] Rao, S. P., Wenzel, A. R., and Oncley, P. B., "Prediction of Ground Effects on Aircraft Noise," NASA TP 1104, 1978.

[7] Ingard, U., "On the Reflection of a Spherical Sound Wave from an Infinite Plane," *Journal of the Acoustical Society of America*, Vol. 23, No. 3, 1951, pp. 329–335. doi:10.1121/1.1906767

[8] Salomons, E. M., *Computational Atmospheric Acoustics*, Kluwer Academic, Norwell, MA, 2001.

[9] Gee, K. L., Gabrielson, T. B., Atchley, A. A., and Sparrow, V. W., "Preliminary Analysis of Nonlinearity in F/A-18E/F Noise Propagation," *10th AIAA/CEAS Aeroacoustics Conference*, AIAA Paper 2004-3009, 2004.

[10] Gee, K. L., Sparrow, V. W., James, M. M., Downing, J. M., and Hobbs, C. M., "Measurement and Predictions of Nonlinearity in Outdoor Propagation of Periodic Signals," *Journal of the Acoustical Society of America*, Vol. 120, No. 5, 2006, pp. 2491–2499. doi:10.1121/1.2345934

[11] Attenborough, K., "Review of Ground Effects on Outdoor Sound Propagation from Continuous Broadband Sources," *Applied Acoustics*, Vol. 24, No. 4, 1988, pp. 289–319. doi:10.1016/0003-682X(88)90086-2

[12] Blackstock, D. T., "Generalized Burgers Equation for Plane Waves," *Journal of the Acoustical Society of America*, Vol. 77, No. 6, 1985, pp. 2050–2053. doi:10.1121/1.391778

[13] Viswanathan, K., "Does a Model Scale Nozzle Emit the Same Jet Noise as a Jet Engine?," *AIAA Journal*, Vol. 46, No. 2, 2008, pp. 336–355. doi:10.2514/1.18019

[14] Morfey, C. L., and Howell, G. P., "Nonlinear Propagation of Aircraft Noise in the Atmosphere," *AIAA Journal*, Vol. 19, No. 8, 1981, pp. 986–992. doi:10.2514/3.51026

[15] Bass, H. E., Sutherland, L. C., Zuckerwar, A. J., and Blackstock, D. T., "Atmospheric Absorption of Sound: Further Developments," *Journal of the Acoustical Society of America*, Vol. 97, No. 1, 1995, pp. 680–683. doi:10.1121/1.412989

[16] Bass, H. E., Sutherland, L. C., Zuckerwar, A. J., and Blackstock, D. T., "Erratum: Atmospheric Absorption of Sound: Further Developments," *Journal of the Acoustical Society of America*, Vol. 99, No. 2, 1996, p. 1259. doi:10.1121/1.415223

[17] Viswanathan, K., "Recent Advances in Jet Noise Suppression," Invited Presentation at *The International Symposium on Recent Advances in Aeroacoustics and Active Flow-Combustion Control* [CD-ROM], in Honor of Professor Ffowcs–Williams, Jan. 2005.

[18] Viswanathan, K., "An Improved Method for Prediction of Noise from Single Jets," *AIAA Journal*, Vol. 45, No. 1, Jan. 2007, pp. 151–161. doi:10.2514/1.23202

[19] Gee, K. L., Shepherd, M. L., Falco, L. E., Atchley, A., Ukeiley, L. S., Jansen, B. J., and Seiner, J. M., "Identification of Nonlinear and Near-Field Effects in Jet Noise Using Nonlinearity Indicators," AIAA Paper 2007-3653, May 2007.

[20] Fisher, M. J., Harper-Bourne, M., and Glegg, S. A. L., "Jet Engine Noise Source Location: The Polar Correlation Technique," *Journal of Sound and Vibration*, Vol. 51, No. 1, 1977, pp. 23–54. doi:10.1016/S0022-460X(77)80111-9

[21] Viswanathan, K., "Investigation of Noise Source Mechanisms in Subsonic Jets," *AIAA Journal*, Vol. 46, No. 8, 2008, pp. 2020–2032. doi:10.2514/1.34471, ;also see AIAA Paper 2007-3601, May 2007.

[22] Viswanathan, K., "Instrumentation Considerations for Accurate Jet Noise Measurements," *AIAA Journal*, Vol. 44, No. 6, 2006, pp. 1137–1149. doi:10.2514/1.13518

D. Gaitonde
Associate Editor